Estimation of shallow water depth from swell patterns using GF-3 SAR data

Xiaolin Bian (1)(2), Yun Shao (1)(2)(3), Chunyan Zhang (1)(2), Chou Xie (1)(2)(3), Wei Tian (1)(2)

[1] Laboratory of Target Microwave Properties, Deqing Academy of Satellite Applications, Zhejiang 313200, China

[2] Aerospace Information Research Institute, Chinese Academy of Sciences, Beijing 100101, China

[3] University of Chinese Academy of Sciences, Beijing 100049, China

Email:bianxl@radi.ac.cn

Abstract: In this study, we evaluate the feasibility of swell-based bathymetry using Chinese quad-polarization Gaofen-3 (GF-3) synthetic aperture radar (SAR) data. To achieve this purpose, detectable shallow water depths are estimated from the dominant scattering component by using the linear dispersion relation and polarization decomposition. By comparing with the values from an official electronic navigational chart (ENC), the mean absolute and relative error of the results from the scattering mechanisms based method are about 1.39m and 8.89%, respectively. Results indicate that Chinese quad-polarization GF-3 SAR is capable of detecting shallow water depths, and the dominant scattering mechanisms based method is feasible for swell-based bathymetry.

Keywords: Bathymetry, Dispersion relation, Swell waves

1. INTRODUCTION

Detailed shallow water depth information has great significance in human activities such as, safe navigation, and harbor security (Calkoen et al., 2001 , Holland, 2001 , Jackson and Apel, 2004). Traditionally, sonar-based bathymetric soundings provide high precision for sea-bed point measurement. However, factors such as implementation costs, bad weather conditions, and poor costal navigation affect their applications (Calkoen et al., 2001). Several remote sensing technologies, including light detection and ranging (LIDAR) (Costa et al., 2009 , Fernandez-Diaz et al., 2014), optical (Sandidge and Holyer, 1998 , Eugenio et al., 2015), and synthetic aperture radar (SAR) (Brusch et al., 2011 , Alpers and Ingo, 1984 , Yang et al., 2010 , Fan et al., 2011 , Renga et al., 2014 , Pereira et al., 2019), have been suggested for directly and indirectly detecting shallow water depth. The LIDAR- and optical-based methods which depend upon moderately high water clarity detect shallow water depth by estimating the depth of light penetration at various wavelengths to the bottom (up to 20 m) (Pleskachevsky et al., 2011). In contrast, the SAR-based methods are better for bathymetric mapping in cloudy and rainy conditions or in turbid waters (e.g., the coastal regions in the East China Sea and the Yellow Sea) (Bian et al., 2018).

The phenomenon of shoaling waves in SAR images provides useful information for interfering shallow water bathymetry, which is called the swell-based method. Different spaceborne SAR satellites(Bian et al., 2020), including L-band (Boccia et al., 2015), S-band (Bian et al., 2016), C-band (Pereira et al., 2019 , Bian et al., 2018 , Bian et al., 2017 , Mishra et al., 2014), and X-band (Monteiro, 2013 , Brusch et al., 2011 , Pleskachevsky et al., 2011), have been applied to detect shallow water depth based on swell-based methods. This work aims to evaluate the swell-based method proposed by Bian et al. (2017) using GF-3 SAR data.

2. DATA AND METHODS

2.1 Study area and SAR data

The study area is located in Xiapu, Fujian province, China where water depth is shallower than 22 m from ENC. The GF-3 satellite was launched on 9 August 2016 (in China launch on 10 August), developed by the Chinese Academy of Space Technology (CAST). The GF-3 satellite has 12 imaging modes, including spotlight, stripmap and scan, with four polarization capability. The satellite works in an orbit altitude of about 755 km in a sun synchronous orbit in a side looking attitude. Figure 1 displays the collected C-band fine quad-polarization GF-3 images (http://210.72.27.21:8790/SNFFWeb/WebUI/HomePage.jsp) and the polarization decomposition result over the study area. The Freeman-Durden decomposition results (Ps: the power of surface scattering component, Pd: the power of double-bounce scattering component, and Pv: the power of volume scattering component) as shown in Figure 1 (d) shows that color red is dominant, that means the surface scattering is the dominant backscatter mechanism.

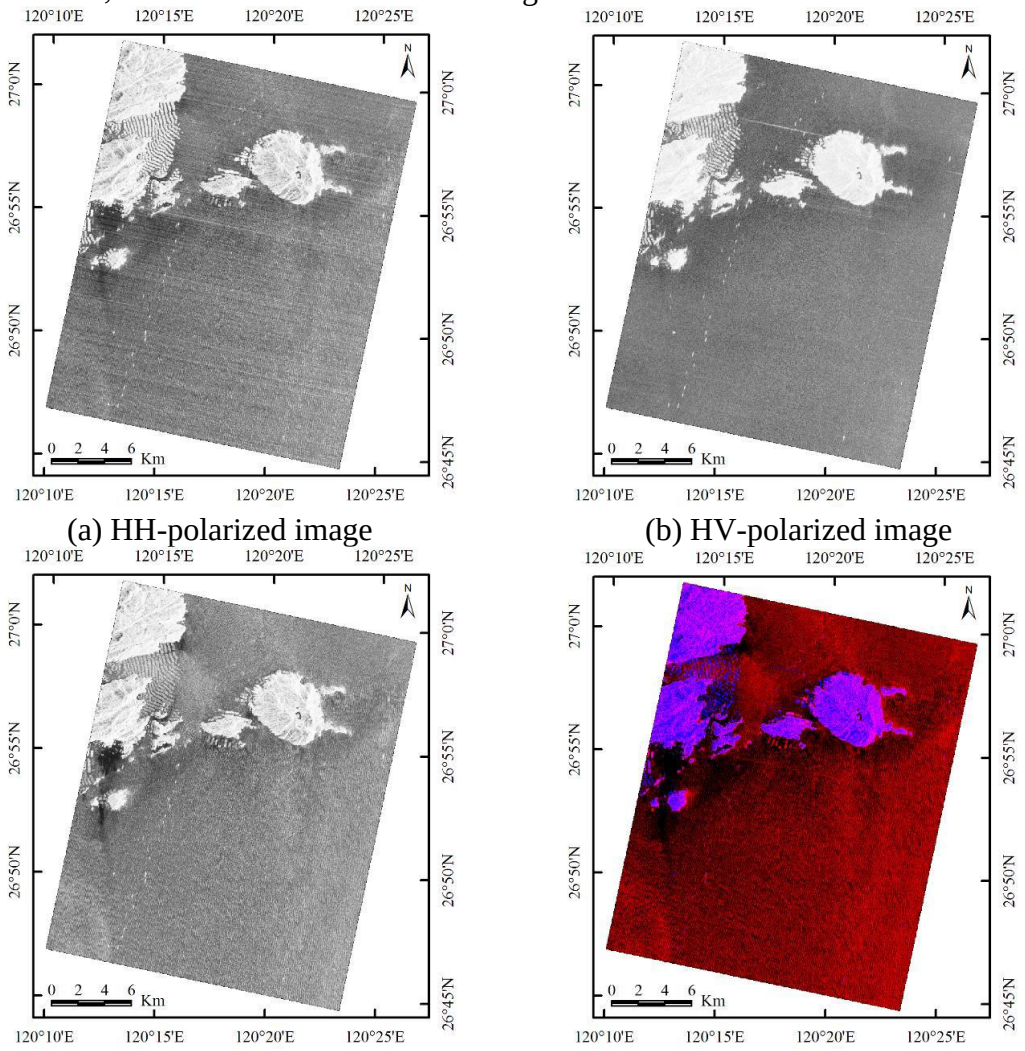

(a) HH-polarized image (b) HV-polarized image

(c) VV-polarized image (d) Color-coded image of the Freeman-Durden decomposition red, Ps; green, Pd; and blue, Pv

Figure 1. The C-band fine quad-polarization GF-3 SAR images and the polarization decomposition result in Xiapu coastal region, Fujian province, China, acquired on October 22, 2017 at 21:56 UTC.

2.2 Linear dispersion relation

The most significant environmental feature of the shallow waters is that water depth is

shallow and change rapidly (Jackson and Apel, 2004). As swell waves travel from deep waters where water depth is larger than half the wavelength to shallow waters where water depth is between 1/20th and half of the wavelength, their wave height increase, speed decrease, length decrease as wave orbits become asymmetrical. The relationship between wave frequency and water depth can be described by the dispersion relation.

If the effect of current (e.g. current velocity less than 0.05m/s) can be neglected, shallow water depth (d) can be estimated from the linear dispersion relation which can be written as follows (Bian et al., 2016):

$$d = \frac{L}{4\pi} ln(\frac{2\pi g+\omega^2 L}{2\pi g-\omega^2 L}) \quad (1)$$

where ω ($\omega = 2\pi/T$, T is the swell period) is the angular wave frequency, g is the gravitational acceleration (9.8 m/s^2), k ($k = 2\pi/L$, L is the wavelength) is the wave number. The required swell wave parameters can be tracked by ray tracing mode, fixed grid mode or the integrated mode by using the fast Fourier transformation (FFT) for swell-based bathymetry (Bian et al., 2016).

3. RESULTS

Figure 2 shows swell wave tracking results which were tracked by fixed grid mode from surface component from Freeman-Durden polarization decomposition using fully polarimetric GF-3 SAR data. Each arrow corresponds to a FFT-box (512×512 pixels) of 2.56 km by 2.56 km, and its length and color mean the value of wavelength and direction means the direction of swell waves. The distance between two arrows is 1.5 km. The swell wave tracking results show a decreasing trend from the southeast to the northwest, and the propagation direction also gradually changes, which is in good agreement with the corresponding water depth distribution from ENC.

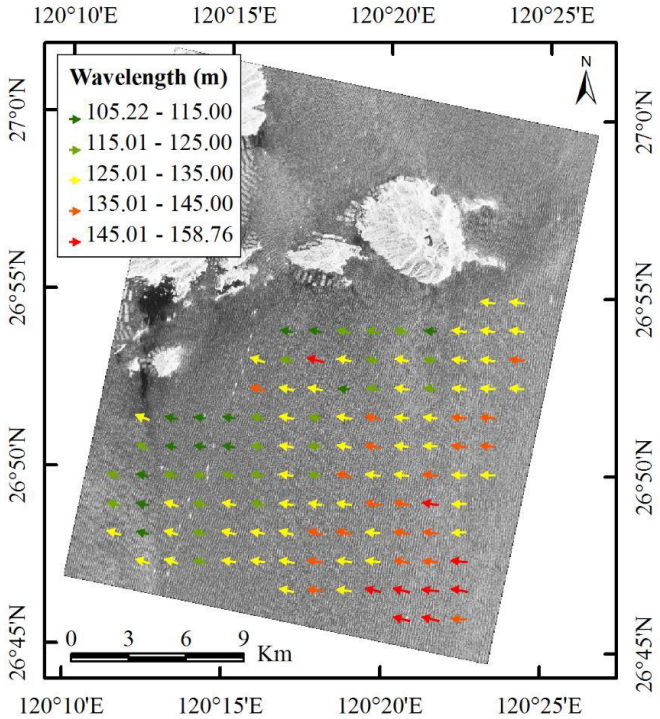

Figure 2. Wave fields map tracked by fixed grid mode from surface component from Freeman-Durden polarization decomposition using fully polarimetric GF-3 SAR data.

Shallow water depths are estimated from the retrieved wavelengths by the linear dispersion relation (Equation (1)). Figure 3 shows the results of swell-based bathymetry from an estimated swell period of 11.2 s. The variation trend of the estimated shallow water depths from co-polarization images and surface component Freeman-Durden polarization decomposition are similar with each other, which is basically consistent with that of ENC. Compared with the estimated shallow water depths from co-polarization images, although the estimated results from cross-polarization image reflects the features of underwater topography, some water depths are overestimated (as shown in Figure 3 (b) the upper left corner and the middle of the bottom part in the effective area).

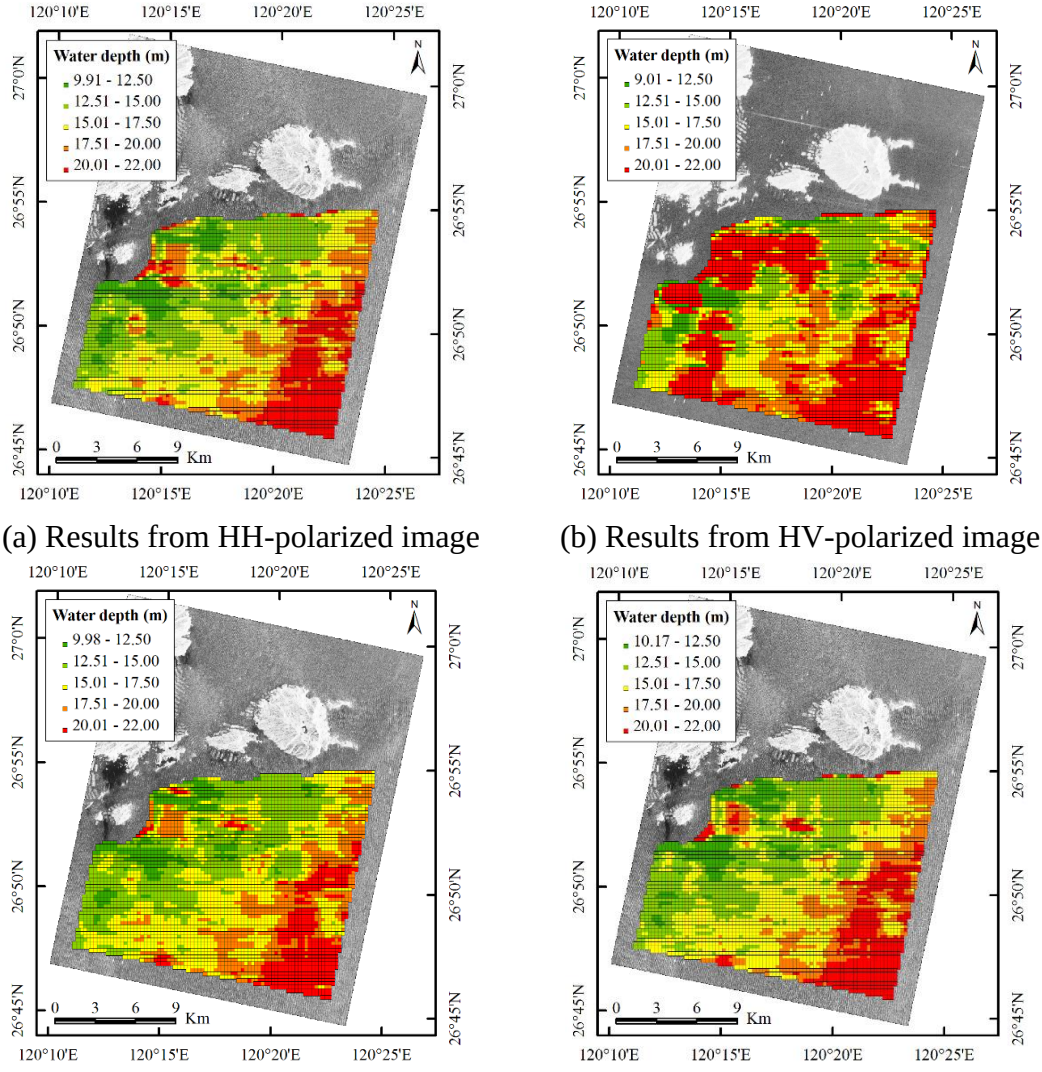

(a) Results from HH-polarized image (b) Results from HV-polarized image

(c) Results from VV-polarized image (d) Results from surface component

Figure 3. Shallow water depths estimated from single polarization and fully polarimetric GF-3 SAR data.

Figure 4 shows the 3D results of shallow water depth estimated from GF-3 polarimetric SAR data based on Freeman-Durden polarization decomposition, and some missing values are interpolated by Kriging. It can be seen from the mapping that the overall change trend of

shallow water depth is basically consistent with that of ENC, showing gradually shallower from southeast to northwest, and the change is relatively gentle, but it shows more detailed topographic information of shallow water than that of ENC used for comparison and analysis.

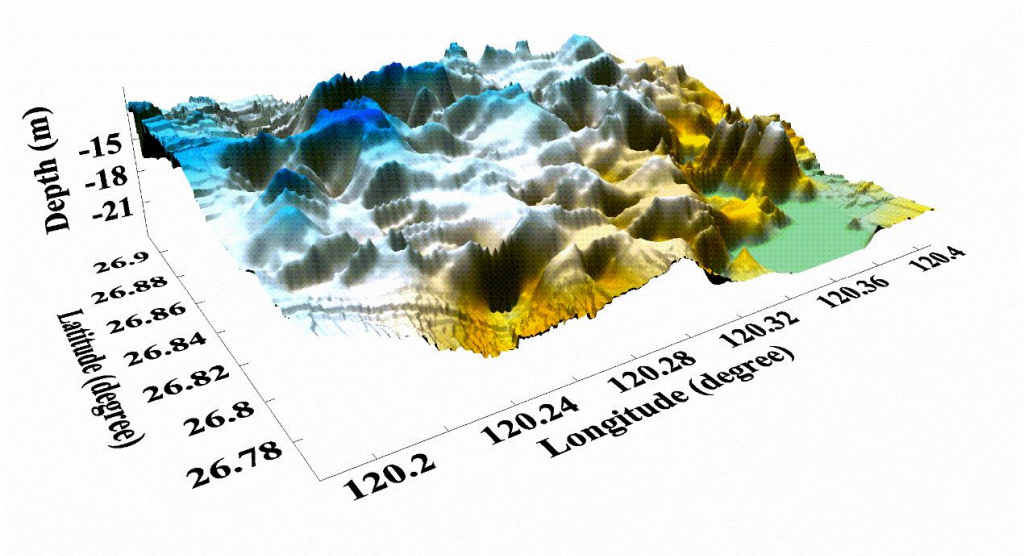

Figure 4. The 3D results of shallow water depth (about 275.0 km^2) from fully polarimetric GF-3 SAR data.

We use the 1:100000 ENC bathymetric data (a total of 86 points) to compare and the mean absolute error (MAE) and the mean relative error (MRE) as indicators to validate the estimated results from GF-3 polarimetric SAR data based on swell-based bathymetry. The detection result based on the dominant scattering component (the scattering component of Freeman Durden polarization decomposition surface) is the best (MAE is 1.80 m and MRE is 11.62%), followed by VV polarization (MAE is 1.95 m and MRE is 12.62%), HH polarization (MAE is 2.01 m and MRE is 13.09%) and cross-polarization (MAE is 3.46 m and MRE is 22.51%). Based on the discrete convolution method proposed by Bian et al. (2018), the detection results after optimization MRE the same as those without optimization, MAE and MRE are 1.39 m and 8.89%, respectively. It is confirmed that the optimization method based on discrete convolution can improve the detection accuracy of shallow water depth. Although the visual interpretation of HH polarimetric SAR image contains periodic speckle noise, according to the characteristics of FFT transform, the detection results are not obviously affected by speckle noise, which is close to VV polarization.

4. CONCLUSIONS

In this work, we evaluate the feasibility of China's first C-band GF-3 SAR satellite to detect shallow water depth based on linear dispersion relation. The results indicate that GF-3 SAR has the ability to detect underwater topography in shallow waters. Based on our comparison analyses, the scattering mechanisms based method has better accuracy (MAE:1.39 m and ARE: 8.89%) than that from single polarization SAR data. Under the conditions of moderate wind speed and medium incidence angle, the combination of optimization method based on discrete convolution and polarization decomposition based on dominant scattering mechanism can effectively improve the detection accuracy of underwater topography in shallow waters.

References

Alpers W, Ingo H, 1984. A theory of the imaging mechanism of underwater bottom topography by real and synthetic aperture radar. J. Geophys. Res. Oceans, 89: 10529–10546.

Bian X, Shao Y, Tian W, et al., 2017. Underwater Topography Detection in Coastal Areas Using Fully Polarimetric SAR Data. Remote Sens., 9: 560.
Bian X, Shao Y, Tian W, et al., 2016. Estimation of Shallow Water Depth Using HJ-1C S-band SAR Data. J. Navig., 69: 113-126.
Bian X, Shao Y, Wang S, et al., 2018. Shallow Water Depth Retrieval From Multitemporal Sentinel-1 SAR Data. IEEE J. Sel. Topics Appl. Earth Observ. Remote Sens., 11: 2991-3000.
Bian X, Shao Y, Zhang C, et al., 2020. The feasibility of assessing swell-based bathymetry using SAR imagery from orbiting satellites. ISPRS J. Photogramm. Remote Sens., 168: 124-130.
Boccia V, Renga A, Moccia A, et al., 2015. Tracking of Coastal Swell Fields in SAR Images for Sea Depth Retrieval: Application to ALOS L-Band Data. IEEE J. Sel. Topics Appl. Earth Observ. Remote Sens., 7: 3532-3540.
Brusch S, Held P, Lehner S, et al., 2011. Underwater bottom topography in coastal areas from TerraSAR-X data. Int. J. Remote Sens., 32: 4527-4543.
Calkoen C J, Hesselmans G H F M, Wensink G J, et al., 2001. The Bathymetry Assessment System: efficient depth mapping in shallow seas using radar images. Int. J. Remote Sens., 22: 2973-2998.
Costa B M, Battista T A, Pittman S J, 2009. Comparative evaluation of airborne LiDAR and ship-based multibeam SoNAR bathymetry and intensity for mapping coral reef ecosystems. Remote Sens. Environ., 113: 1082-1100.
Eugenio F, Marcello J, Martin J, 2015. High-Resolution Maps of Bathymetry and Benthic Habitats in Shallow-Water Environments Using Multispectral Remote Sensing Imagery. IEEE Trans. Geosci. Remote Sens., 53: 3539-3549.
Fan K, Huang W, Lin H, et al., 2011. Shallow water depth retrieval from space-borne SAR imagery. Journal of Oceanogr., 67: 405-413.
Fernandez-Diaz J C, Glennie C L, Carter W E, et al., 2014. Early Results of Simultaneous Terrain and Shallow Water Bathymetry Mapping Using a Single-Wavelength Airborne LiDAR Sensor. IEEE J. Sel. Topics Appl. Earth Observ. Remote Sens., 7: 623-635.
Holland T K, 2001. Application of the linear dispersion relation with respect to depth inversion and remotely sensed imagery. IEEE Trans. Geosci. Remote Sens., 39: 2319-2319.
Jackson C R, Apel J R, 2004. Synthetic Aperture Radar Marine User's Manual [M]. NOAA; Washington, DC.
Mishra M K, Ganguly D, Chauhan P, et al., 2014. Estimation of Coastal Bathymetry Using RISAT-1 C-Band Microwave SAR Data. IEEE Geosci. Remote Sens. Lett., 11: 671-675.
Monteiro F, 2013. Advanced Bathymetry Retrieval from Swell Patterns in High-Resolution SAR Images [M]. University of Miami.
Pereira P, Baptista P, Cunha T, et al., 2019. Estimation of the nearshore bathymetry from high temporal resolution Sentinel-1A C-band SAR data - A case study. Remote Sens. Environ., 223: 166-178.
Pleskachevsky A, Lehner S, Heege T, et al., 2011. Synergy and fusion of optical and synthetic aperture radar satellite data for underwater topography estimation in coastal areas. Ocean Dynam., 61: 2099-2120.
Renga A, Ruflno G, D'errico M, et al., 2014. SAR Bathymetry in the Tyrrhenian Sea by COSMO-SkyMed Data: A Novel Approach. IEEE J. Sel. Topics Appl. Earth Observ. Remote Sens., 7: 2834-2847.
Sandidge J C, Holyer R J, 1998. Coastal Bathymetry from Hyperspectral Observations of Water Radiance. Remote Sens. Environ., 65: 341-352.
Yang J, Zhang J, Meng J, 2010. A detection model of underwater topography with a series of SAR images acquired at different time. Acta Oceanol. Sinica, 29: 28-37.